Sources of water vapor to economically relevant regions in Amazonia and the effect of deforestation

Telmo Cosme António Sumila*, Gabrielle Ferreira Pires, Vitor Cunha Fontes, Marcos Heil Costa

Department of Agricultural Engineering, Federal University of Viçosa, Av. P. H. Rolfs, s/n, Viçosa, MG, 36570-900, Brazil

* Permanent affiliation: National Institute of Meteorology of Mozambique

Corresponding author address: Gabrielle Ferreira Pires, Department of Agricultural Engineering, Federal University of Viçosa, Av. P. H. Rolfs, s/n, Viçosa, MG, 36570-000, Brazil.

Email: gabrielle.pires@ufv.br

Manuscript accepted for publication at Journal of Hydrometeorology

March 10, 2017

Abstract

The Amazon rainforest helps regulate the regional humid climate. Understanding the effects of the Amazon deforestation is important to preserve not only the climate, but also economic activities that depend on it, in particular agricultural productivity and hydropower generation. This study calculates the source of water vapor contributing to the precipitation on economically relevant regions in Amazonia according to different scenarios of deforestation. These regions include the state of Mato Grosso, which produces about 9% of the global soybean production, and the basins of the Xingu and Madeira, with infrastructure under construction that will be capable to generate 20% of the electrical energy produced in Brazil. The results show that changes in rainfall after deforestation are stronger in regions nearest to the ocean, and indicate the importance of the continental water vapor source to the precipitation over southern Amazonia. In the two more continental regions (Madeira and Mato Grosso), decreases in the source of water vapor in one region were offset by increases in contributions from other continental regions, whereas in the Xingu basin, that is closer to the ocean, this mechanism did not occur. As a conclusion, the geographic location of the region is an important determinant of the resiliency of the regional climate to deforestation induced regional climate change. The more continental the geographic location, the less climate changes after deforestation.

Key Words: Amazonia, deforestation, climate change

1. Introduction

For several decades the Amazon rainforest has been struck by deforestation regardless of its important contribution in maintaining biodiversity, water resources, climate and terrestrial carbon storage (Ladle et al. 2010; Joetzjer et al. 2013; Drumond et al. 2014). Although large areas remain intact, the forest loss is dramatic especially in the "arc of deforestation" along the southern and eastern edges. From 2000 to 2011 the area of the Amazon forest removed grew from approximately 530,000 km^2 to about 680,000 km^2 (Sampaio et al. 2007; Lapola et al. 2013). However, the pressure to reduce rates of deforestation in the Amazon has increased both nationally and internationally (Ladle et al. 2010), and deforestation rates (km^2 deforested per year) declined 77% in recent years compared with the deforestation rates in the reference years 1995-2005, making Brazil largely responsible for the reduction of global tropical deforestation (Nobre 2009; Hansen et al. 2013). Depending on the extent, deforestation can affect climate from the mesoscale to the regional scale, and possibly have global consequences (Roy and Avissar 2002; Costa and Foley 2000; Chagnon and Bras 2005; Costa and Pires 2010; Pires and Costa 2013).

The Amazon forest is an important source of moisture to the regional atmosphere (Spracklen and Garcia-Carreras, 2015). Deforestation, in addition to reducing the flux of water vapor into the atmosphere, can also change the convection over the Amazon Basin, leading consequently to changes in the regional circulation systems such as the Bolivian High, the subtropical Jet stream, the South American Low Level Jets (SALLJs), trade winds and the upper tropospheric cyclonic vortices center near the northeast coast of Brazil (Marengo et al. 2012; De Almeida et al. 2007; Misra 2008; Carvalho et al. 2010). Moisture tracing by Spracklen et al. (2012) indicates that deforestation of 40% of the Amazon results in 12% reduction in rainfall in the rainy season and 21% reduction in precipitation in the dry season throughout the Amazon basin, but the impact may extend to 4% reduction in rainfall in the Rio de La Plata basin thousands of kilometers south of the Amazon. Keys et al. (2016) also indicate that such impacts are more drastic during the dry season in Mato Grosso (southern Amazon). Moreover, Costa and Pires (2010) and Butt et al. (2011) concluded that there is an increase in the duration of the dry season and a delay in the beginning of the rainy season in some regions of the Amazon associated with progressive deforestation.

The main atmosphere flux of water vapor into the basin comes from trade winds: 64% and 34% of the moisture influx enters through the eastern and northern border respectively (Costa and Foley 1999; Paegle and Mo 2002; Carvalho et al. 2010; Durán-Quesada et al. 2012). Satyamurty et al. (2012) studied the sources and sinks of moisture for the Amazon Basin and showed that 68% of the Amazon precipitation is accounted for by the moisture transport from the North and South Tropical Atlantic Ocean, leaving 32% of precipitation to inland sources.

Several studies define the concept of water vapor recycling as the contribution of the local evapotranspiration of some region (e.g., the Amazon basin) on precipitation at any point within the same region (Eltahir and Bras, 1994; Eltahir, 1996). Martinez and Dominguez (2014) calculated that the percentage of water recycled in the Amazon Basin is between 20 and 30%, even considering that recycling has significantly different patterns depending on the space and seasonality. During part of the year, the east-west gradient dominates the water vapor recycling, consistent with the predominance of easterly winds in the basin. The opposite occurs during the southern hemisphere summer, when the south-north gradient is most influenced by southward migration of the Intertropical Convergence Zone (ITCZ), the onset of the South America Monsoon System and dominance of northerly winds in most of the Amazon.

An initial analysis of the interplay between the influences of forests on discharge found that projected rates and spatial patterns of future deforestation could significantly diminish water flow in six of the 10 major Amazon tributaries (Coe et al. 2009). The biggest effect of simulated future deforestation on hydrology was found on the Xingu River basin, where discharge under deforestation scenarios is estimated to decline 11–17% (Coe et al. 2009; Stickler et al. 2013). Furthermore, Stickler et al. (2013) found that, as regional forest cover declines, simulated rainfall within the Xingu basin also drops, thereafter reducing discharge by 6-13% under a scenario of 15% regional deforestation, and by 30-36% under a scenario of 40% regional deforestation compared with reference scenario simulation. If deforestation proceeds as predicted (Soares-Filho et al. 2006) within both the Xingu and Amazon basins and simulated effects of forests on rainfall are taken into consideration, mean annual power generation potential could decline to ~25% of maximum installed capacity (Stickler et al. 2013). According to some studies (e.g., Costa, 2005; Coe et al. 2009), deforestation has different effects at the micro/meso-scale and at the large scale. At micro-scale to meso-scale, deforestation generally results in decreased evapotranspiration and increased runoff and discharge. At the large-scale, atmospheric feedbacks may significantly reduce precipitation regionally and, if larger than the local evapotranspiration changes, may decrease water yield, runoff and discharge.

In addition to the hydroelectric sector, the agricultural sector is largely influenced by some forms of land use leading to the degradation of the climate regulation service provided by the natural ecosystems (Foley et al. 2005; Lawrence and Vandecar 2015). Oliveira et al. (2013) simulated a decrease in agricultural yield in Amazonia in scenarios in which climate change due to changes in atmospheric composition and due to deforestation are evaluated together. In sum, large-scale agriculture expansion in

Amazonia may introduce climate feedbacks that would reduce precipitation, leading to negative effects on the agriculture yield.

In this paper, we determine the sources of water vapor to three economically relevant regions for agricultural production (the soybean producing region of Mato Grosso) and for hydroelectric power generation (hydropower plants in Xingu and Madeira basins), and how deforestation affects these sources of water vapor.

2. Data and Methodology

2.1. Background

The abundant rainfall that has permitted tropical rainforest ecosystems has also allowed important economic activities to develop. The long rainy season with frequent rains enabled an intensive agriculture, where two harvests are possible per year, while the large volumes of river water flow created a high potential for the generation of electricity through hydropower plants. Currently, 21.8 million tons of soybeans (9% of the global production) are produced in the intensive cropping systems in Mato Grosso (Pires et al., 2016), while three of the six largest hydropower plants in Brazil are completing construction on two tributaries of the Amazon, the Xingu River and the Madeira River (Figure 1). On the Xingu River, the Belo Monte hydropower plant started operation in 2016 and, when completed (in 2019), will be the third largest of the world, and the second largest of Brazil, with an installed capacity of 11,300 MW. On the Madeira River, two hydropower plants (Santo Antonio and Jirau) are under construction. Santo Antonio will have an installed capacity of 3,600 MW and will be the sixth largest power plant in Brazil, while Jirau will have an installed capacity of 3,750 MW when completed and will be the fifth largest in Brazil. The combined under construction hydropower generation capacity of these two basins is over 18 GW, which corresponds to about 20% of current electric power generation capacity in Brazil (MME, 2016). The Madeira River is also the largest tributary of the Amazon, and if it were not part of the Amazon system, it would be the third largest river of the world, with an annual mean discharge of 50,000 $m^3 s^{-1}$.

2.2. Data used and description of climate scenarios of deforestation

The data used in this study are the results of a numerical experiment using the Community Climate Model version 3 coupled to the Integrated Biosphere Simulator version 2.6.4 (CCM3-IBIS) to evaluate the climate scenarios after various scenarios of progressive deforestation in the Amazon. The model description parallels that of Costa and Pires (2010) as follows in the next section.

2.2.2 Model description

The coupled CCM3-IBIS model (Delire et al., 2002) consists of the National Center for Atmospheric Research (NCAR) Community Climate Model version 3 (CCM3, Kiehl et al., 1998) coupled with an updated version of the Integrated Biosphere Simulator (IBIS) of Foley et al. (1996).

CCM3 is an atmospheric general circulation model with spectral representation of the horizontal fields. In this study, the model operated at the T42L18 resolution (horizontal fields converted to a 2.81°×2.81° grid and 18 levels in the vertical), with a 20-min time step. T42L18 resolution leads to a reasonable representation of the major climate features and most large and synoptic scale processes of the Amazon, but it is not sufficient to represent sub-synoptic or mesoscale phenomena (Costa and Pires, 2010).

IBIS represents two dynamic vegetation layers (i.e. trees and short vegetation), but in this experiment the vegetation cover was fixed through the duration of the simulations. The land surface physics and canopy physiology are also calculated at the

T42 resolution and a 20-min time step, as well as the atmospheric model (Costa and Pires, 2010). The rainforest representation in IBIS was calibrated against flux data using data from the Large-Scale Biosphere Experiment in Amazonia (LBA) (Imbuzeiro, 2005).

2.2.3 Deforestation scenarios

The experiment evaluated deforestation scenarios for the Amazon ranging from 0 to 100% of the Pan-Amazonia. The initial range of Amazon deforestation scenarios (10–30%) is based on Soares-Filho et al.'s (2006) scenarios. The scenarios beyond 30% were developed considering two main conditions for Amazon deforestation: the presence of roads and protected areas, as described in Pires and Costa (2013). The authors assumed that the presence of roads is an enabler of deforestation, while protected areas limit deforestation of the Amazon rainforest. Deforestation represents the substitution of tropical forest with pasture in the entire grid cell, which is parameterized according to Costa et al. (2007). In this study, we used only the results of deforestation scenarios of 0 (F0), 20% (F20), 40% (F40) and 60% (F60) (Figure 2) of the Amazon forest; whereas part of the remaining 40% of the rainforest matches protected areas and indigenous territories that are unlikely to be deforested.

The scenarios were then implementd in CCM3-IBIS to generate the climate scenarios. The simulations were run for 50 years, from 1951-2000, with the observed Sea Surface Temperature (SST) for the same period. The simulations included five ensembles (simulations started at 17, 18, 19, 20 or 21 January) and atmospheric CO_2 concentrations were fixed at 380 ppmv. The first 10 years were left for the model to approach a steady state, specifically in relation to soil moisture, while the last 40 years were used to define the average climate. Then, we calculated the source and destination of water vapor on each ensemble member and averaged the final results to plot the Figures presented in this work.

2.3. Theory to compute the source and destination of water vapor

Several studies described methods for the identification of sources and destinations of water vapor contributing to precipitation events by tracing the origin of the spatial and temporal movement of an air mass at each pixel in numerical model grid. According to Gimeno et al. (2012), the methods are categorized into Analytical Box Methods, Numeric Water Vapor Tracers and Physical Water Vapor Tracers (isotopes). The first method is relatively simple and can be calculated offline, the second is usually calculated during model simulations, which is computationally more expensive, and the latter is often used to validate other methods. Some examples are the bulk method described by van der Ent et al. (2010), the isotopic analysis described by Henderson-Sellers et al. (2002) and the Lagrange integral described by Stohl and James (2004, 2005) and Gimeno et al. (2010). In this study, we used the bulk method described by van der Ent et al. (2010) to estimate the water cycle in the air from the source (evapotranspiration) to the destination (precipitation) and vice versa making use of techniques of numerical modeling. This method identifies the sources of evapotranspiration contributing to the occurrence of precipitation by tracing the air flow backwards and/or forwards in time through the analysis of grid model data. The method is based on the use of two-dimensional data of precipitation and evapotranspiration and three-dimensional data of wind and water vapor, and can be applied to field data or data generated by a climate model. Ideally, data should be of high temporal-resolution (hourly or less), however monthly fields can be used if the covariance terms are available. This method assumes that (i) every molecule of water vapor within the tropospheric column is equally likely to precipitate; (ii) the water evaporated from the surface mixes uniformly through the atmospheric column and does not precipitate in the same pixel – the latter may incur in an error of ~9.4% according to van der Ent and Savenije (2011) (first equation in Table 1) and Eltahir and Bras (1994, 1996) (equation in Figure 6); (iii) the water vapor portion may fall from any level and can be back to a random level.

The method makes use of relatively simple calculation and is computationally less expensive than other methods. However, the atmospheric column "well-mixed" assumption that leads to a 2-D tracing of the atmospheric moisture has been criticized by Groessling and Reick (2013), who argue that it may lead to large errors for neglecting wind shear in the atmosphere. Yet, for the Amazon region, the authors considered that the method leads to reasonable results in January. On the other hand, the authors show that in July it may lead to unrealistic precipitation of Amazon evapotranspiration in the Pacific Ocean, but this time of the year is not in the scope of this study.

From the conservation of water vapor:

$$\frac{\partial \mathbf{F}_u}{\partial x} + \frac{\partial \mathbf{F}_v}{\partial y} = E - P \tag{1}$$

Where F_u and F_v are the horizontal water vapor fluxes in the zonal and meridional directions respectively, E is the evapotranspiration and P is the precipitation. The water vapor flux integrated in the entire atmospheric column of each pixel is given by the following expressions:

$$\mathbf{F}_u = \frac{W_u}{\mathbf{g}} \int_{p=0}^{ps} \overline{\mathbf{u}q}\, dp, \text{ where } \quad \overline{\mathbf{u}q} = \bar{\mathbf{u}}\,\bar{q} + \overline{\mathbf{u}'q'} \tag{2}$$

$$\mathbf{F}_v = \frac{W_v}{\mathbf{g}} \int_{p=0}^{ps} \overline{\mathbf{v}q}\, dp, \text{ where } \quad \overline{\mathbf{v}q} = \bar{\mathbf{v}}\,\bar{q} + \overline{\mathbf{v}'q'} \tag{3}$$

$\bar{\mathbf{u}}$, $\bar{\mathbf{v}}$, $\bar{q}$, $\overline{\mathbf{u}'q'}$, $\overline{\mathbf{v}'q'}$ are zonal and meridional mean wind speed, mean specific humidity and their covariance, respectively (van der Ent et al. 2010). W_u and W_v are the horizontal widths perpendicular to the directions of the zonal and meridional moisture flux respectively, **g** is the acceleration due to gravity equal to 9.80616 m.s^{-2} and ps is the surface pressure. Isolating P in the balance Equation (1) we have:

$$P = E - \frac{\partial \mathbf{F}_u}{\partial x} - \frac{\partial \mathbf{F}_v}{\partial y} \tag{4}$$

From Equation (4) one can recursively calculate the moisture proportions corresponding to each contributing factor. The average flux of the neighbor pixels will result in an average flux at the interface of the pixel in question, which can be positive or negative, and by logical analysis will be the input or output of each grid pixel, thereby determining the sources and destinations of precipitated and evaporated water vapor in the study region.

As an example of the calculations of sources of water vapor to a given pixel (i,j) in month t described above, the contribution of a neighbor pixel (i-1,j), $C_{i-1,j}$, is given by Equation (5):

$$C^t_{i-1,j} = \frac{uq^t_{i-1,j}}{q^t_{in}} P^t_{i,j} \tag{5}$$

Where $uq^t_{i-1,j}$ is the zonal water vapor transport from pixel (i-1,j) to pixel (i,j), q^t_{in} is the total moisture advected to pixel (i,j) from the neighbor pixels and $P^t_{i,j}$is the precipitation in pixel (i,j) in month t.

Similar calculation are performed for all neighbor pixels to account for water vapor input to pixel (i,j) in the zonal and meridional directions.

3. Results and Discussion

3.1. Climatology of precipitation patterns in South America and evapotranspiration in Amazonia

The wet season in tropical South America starts in late September/early October, is fully developed during December to February and retreats in late April or early May (Silva and Carvalho 2007; Richter and Mechoso 2007; Silva and Kousky 2012; Marengo et al. 2012). During the wet season, the wettest region in South America follows the NW to SE path, from Colombia to the southeastern Brazil (Figure 3). In most of the South America Monsoon Systems (SAMS) region, precipitation peaks in the southern hemisphere spring and summer (September-October-November – SON and December-January-February – DJF), while in the north of the equator the wet season occurs in the southern hemisphere winter (Vera et al. 2005; Marengo et al. 2012). The largest contrast of rainfall between summer and winter is in central South America (Bolivia and Central-western Brazil) with almost all rainfall occurring from October to March (Figures 3b, 3e and 3k). A comparison between the simulated and observed (CRU - Climate Research Unit) data indicates that the simulations are representative of the climatology of precipitation. Although the seasonal rain patterns are similar to the observed, in the rainiest regions the simulated climate overestimates the observed results between 2 to 6 mm day^{-1} (about 28% to 43%) over most of the central-western region of Brazil, south of the Amazon, some regions of Pará, Tocantins, Bahia, and southeastern Bolivia (Figure 3). In the same season, in northern Amazonia, precipitation may be overestimated by more than 6 mm day^{-1} (Figure 3l). At the beginning of the dry season (March-April-May trimester, or MAM), the simulated precipitation is well simulated over the region of interest, but underestimates the observed precipitation by about 2 to 6 mm day^{-1} in northern South America and southern Brazil (Figure 3f). In the dry season months of June-July-August (JJA), simulations consistently represent the dry season that happen in the region of interest (Figures 3g-i). For the onset of the rainy season (SON), the overestimation of the simulated data dominates in most of the Amazon (Figure 3l).

In addition, CCM3-IBIS tends to overestimate annual mean evapotranspiration in most of the analyzed sites in Amazonia, except for Santarém (Table 1).

3.2. Source of water vapor

Our analysis is concentrated in the two seasons SON and DJF, when soybean crops develop. SON are also the most critical months when change in the hydropower generation are expected. In the case of all three dams analyzed, the lakes formed are relatively small, and insufficient to keep the hydropower plant running at maximum capacity during the dry season. From previous studies using the same model (Costa and Pires, 2010), we expect a late onset of the rainy season during the SON trimester, thus making the analysis of this period critical under deforestation conditions.

Figures 4, 5 and 6 show the vertically integrated water vapor transport for the F0 scenario, and the source of water vapor that precipitates on the Xingu, Madeira and soybean producing regions, respectively, for the scenario F0, and anomalies for the scenarios F20, F40 and F60. In these figures, the sum of all pixels in the map is equal to the amount of precipitation inside the basin. In addition, while interpreting these figures the reader should keep in mind that rather than showing the ocean contribution in a spatially explicit way, here we chose to condense all ocean contributions as originating from the land-surface grid cell directly adjacent to the ocean.

The Xingu basin is relatively close to the ocean, which indicates that most of the water vapor that precipitates inside the basin was evaporated from the Atlantic Ocean (Figures 4b and 4k). During SON, the wind and water vapor transport is typically easterly (Figure 4a), while in DJF it is typically from northeast (Figure 4j). However, in both cases, the air passes over highly deforested land. Indeed, most of deforestation on the 20% scenario happens upwind of the Xingu basin (Figure 2). As a consequence, the deforested regions contribute less water vapor to the precipitation over the Xingu basin (Figures 4c and 4l). From the circulation patterns, the additional deforestation in the F40 and F60 scenarios do not cause additional reduction in rainfall over the Xingu basin (Figures 4d, 4e, 4m, 4n), as it happens mostly downwind of the basin.

The Madeira basin is a large region located inland, on the southwest of the Amazon basin, and relatively close to the Andes (Figure 5). Contrary to the Xingu basin, the humid air crosses a large portion of the continent before precipitating on the Madeira basin (Figure 5a and 5j). In SON, most of water vapor that precipitates in the basin has evaporated either inside it or nearby (Figure 5b), while during DJF, the contribution from the Atlantic Ocean is larger. Most importantly, the main air trajectory, mostly parallel to the equator and turning to SE before arriving at the Madeira basin, crosses a region with little deforestation in all scenarios analyzed. For all three deforestation levels and both seasons analyzed, reductions in rainfall are in the range of 3-5 mm/month, or about 4%.

The soybean producing region in Mato Grosso is to the south and to the west of the Xingu River basin, and between the two other basins analyzed (Figure 1). Because of this intermediary geographical position, the air trajectory to the region has elements from the two previous cases. In SON, air comes mainly from the east, and turns to SW before entering the soybean area (Figure 6a), and most of the water vapor that precipitates on this region has evaporated either nearby or in the ocean. Decreases in precipitation for the three deforested scenarios are in the range of 22 to 27 mm/month (13-16%). Most of the decreases in the source of water vapor that contributes to the precipitation over the region is from nearby pixels (Figures 6c-6e). In scenario F20, half of these main contributing pixels are deforested and the other half are still forested (Figure 2), but the fraction of deforested pixels increase proportionally in the F40 and F60 scenarios. During DJF in the scenario F20, air comes mainly from northeast and east, and crosses heavily deforested regions to the NE of the region. During this season, the source of water vapor shifts, decreasing from the pixels NE of the region, but increasing to the E of the region (Figure 6l, and the total change in rainfall is -12 mm/month (~5%). For higher deforestation scenarios (F40 and F60), apparently competing mechanisms set in, and although the same pattern of shifting the source of water vapor is still observed, the magnitude of the changes is much smaller, and the change in precipitation is close to zero. We should note, however, that in all three cases, the change in rainfall is very small (< 5%), and we attribute this small change to the continentality of the soybean producing region.

3.3. Impacts on economically relevant regions

The decrease in moisture advected from the Amazon to the Xingu basin and the Mato Grosso soybean producing region after deforestation has the potential to cause significant impacts on hydropower generation and agriculture output.

Overall, annual mean power generated at Belo Monte decreases significantly from changes in rainfall in the first 20% of deforestation, when it decreases by about 29%, and then remains relatively constant for higher levels of deforestation (Figure 7-a). This is strong evidence of how this region is dependent on vegetation cover to provide sufficient levels of precipitation, and consequently runoff, to the Belo Monte hydropower plant

The changes on soybean yield according to deforestation depends on the actual planting date (Pires et al., 2016). Here we show results for the planting date September 25, one of the earliest possible planting dates, but which usually allows two crops to be harvested during the same growing season. It is important to highlight that the effects of changes in rainfall is soy productivity may be stronger in planting dates in the transition months from the dry to the wet season (S-O) than in later dates (N-D) (Bagley et al., 2012; Pires et al., 2016).

We consider as the reference the Mato Grosso soybean production in 2012, as in Dias et al. (2016). From the reference production, soybean output could decrease by 2 million tons in the most severe deforestation scenario (Figure 7-b), which is roughly 10% of the current production. This is strong indication that large scale agricultural expansion in Amazonia may compromise ecosystem services it relies on (Oliveira et al., 2013; Pires et al., 2016).

4. Discussion and Conclusions

Regardless of the limitations in the 2-D moisture tracking method described here, the general patterns of changes in water vapor distribution after deforestation is in line with previous studies, such as Henderson-Sellers et al., (2002), Diermeyer and Brubaker (2007), van der Ent et al. (2010), Goessling and Reick (2012) and Keys et al. (2016). Moreover, our results show that changes in rainfall are stronger when the deforested regions are closer to the Atlantic Ocean. In addition, changes are much stronger during SON than during DJF. For the Xingu, rainfall decreases by 32% to 36% in SON and by 2% to 8% in DJF. For the soybean producing region, rainfall decreases by 13% to 16% in SON and by 0 to 5% in DJF. For the Madeira basin, rainfall decreases by ~5% in SON and by ~3% in DJF.

These results indicate the importance of the continental water vapor source, and consequently the vegetation cover, to the precipitation over southern Amazonia, corroborating previous studies (Spracklen et al., 2012; Spracklen et al., 2015; Swann et al., 2015; Keys et al., 2016), and the impacts these changes in deforestation may have in human activity (Oliveira et al., 2013; Stickler et al., 2013; Pires et al., 2016). In two cases (Madeira and Mato Grosso), decreases in the source of water vapor in one region were offset by increases in contributions from other continental regions, whereas in the Xingu basin, that is closer to the ocean, this mechanism did not occur.

These results also confirm the results of Costa and Pires (2010), who indicated that the effects of deforestation are stronger during the onset of the rainy season (SON) than when the season is fully developed (DJF). According to Costa and Pires (2010), during the transition from the dry season to the wet season most of the moisture provided to the atmosphere is from the local evapotranspiration and moisture convergence is small. Deforestation causes important reductions in evapotranspiration and does not significantly decrease moisture convergence over the deforested area. The reduction in evapotranspiration after the deforestation is related to the increased albedo, reduced rooting depth, reduced leaf area and reduced turbulence of the pasture over the rainforest/cerrado (Costa, 2005). In the end of dry season the reduced rooting depth is probably the most significant ecological factor. On the contrary, during the peak of the rainy season, evapotranspiration is similar for both types of land cover (forest/deforested), as the rooting depth is secondary during periods of frequent rainfall events.

As a consequence of this mechanism, farmers in the soybean producing region may expect less rainfall in the transition months SON, or even a delay in the onset of the rainy season, as deforestation progresses, which has already been observed in Rondônia (Butt et al. 2011). They can adapt to this type of climate change by delaying their sowing date to late October and November.

The hydropower to be generated by the power plants on the Madeira River are relatively less sensitive to any climate changes due to deforestation. On the other hand, and confirming the results of Stickler et al. (2013), the power generated by the Belo Monte dam on the Xingu River is probably very sensitive to changes in rainfall in all the deforestation scenarios assessed, in particular during SON, when the lakes formed are relatively small, and insufficient to keep the hydropower plant running at maximum capacity.

Roughly, hydropower generation in Belo Monte may decrease by 28% and Mato Grosso soybean output may decrease by 10% in drastic deforestation scenarios. It is important to highlight that this a permanent service provided by the rainforest, and reducing it by deforestation has effects on every year after deforestation.

We have analyzed the effects of deforestation on the sources of moisture and precipitation on regions that have significant economic activities that depend on rainfall. We conclude that the geographic location of the region is an important determinant of the resiliency of the regional climate to deforestation-induced regional climate change. The more continental the geographic location, the more resilient the climate is to deforestation, and the impacts of climate change on the economic activities developed there should also be smaller. Further studies will quantify the effects of deforestation on these economic activities.

Acknowledgments

This work was supported by the World Bank (contract 7172826) and by Conselho Nacional de Desenvolvimento Científico e Tecnológico (CNPq).

References

Bagley, J. E., Desai, A. R., Dirmeyer, P. A., Foley, J. A. 2012. Effects of land cover change on moisture availability and potential crop yield in the world's breadbaskets. Environmental Research Letters, 7(1), 014009.

Butt, N., P. A., De Oliveira, and M. H. Costa, 2011: Evidence that deforestation affects the onset of the rainy season in Rondonia, Brazil. J. Geophys. Res., 116, D11, D11120, doi: 10.1029/2010JD015174.

Carvalho, L. M. V., A. E. Silva, C. Jones, B. Liebmann, P. L. S Dias, and H. R. Rocha, 2010: Moisture transport and intraseasonal variability in the South America monsoon system. Climate Dyn., 36, 9-10, 1865–1880, doi: 10.1007/s00382-010-0806-2.

Chagnon, F. J. F., and R. L. Bras, 2005: Contemporary climate change in the Amazon. Geophys. Res. Lett., 32, 1–4, doi: 10.1029/2005GL022722.

Coe, M. T., M. H. Costa, and B. S. Soares-Filho, 2009: The influence of historical and potential future deforestation on the stream flow of the Amazon River – Land surface processes and atmospheric feedbacks. J. Hydrol., 369, 1-2, 165–174, doi:10.1016/j.jhydrol.2009.02.043.

Costa, M. H., and J. A. Foley, 1999: Trends in the hydrologic cycle of the Amazon Basin.J. Geophys. Res., 104, D12, 14189, doi: 10.1029/1998JD200126.

Costa, M. H., and J. A. Foley, 2000: Combined effects of deforestation and doubled atmospheric CO2 concentrations on the climate of Amazonia. J. Climate, 13, 18–34, doi: 10.1175/1520-04442(2000)13.

Costa, M.H.. 2005: Large-scale hydrological impacts of tropical forest conversion. Forests, Water and People in the Humid Tropics, M. Bonell, L. A. Bruijnzeel, Eds. Cambridge University Press, 590-597.

Costa, M.H., Yanagi, S.N.M., Oliveira, P.J., Ribeiro, A., Rocha, E.J.P. 2007. Climate change in Amazonia caused by soybean cropland expansion, as compared to caused by pastureland expansion. Geophysical Research Letters 34: L07706, DOI: 10.1029/2007GL029271.

Costa, M. H., and G. F. Pires, 2010: Effects of Amazon and Central Brazil deforestation scenarios on the duration of the dry season in the arc of deforestation. I. J. Climatol., 30, 13, 1970-1979, doi: 10.1002/joc.2048.

Costa,M.H., Biajoli, M.C., Sanches, L., Malhado, A.C.M., Hutyra, L.R., da Rocha, H.R., Aguiar, R.G. and deAraújo, A.C. 2010. Atmospheric versus vegetation controls of Amazonian tropical rain forest evapotranspiration: Are the wet and seasonally dry rain forests any different?, J. Geophys. Res., 115, G04021, doi:10.1029/2009JG001179.

De Almeida, R. A. F., P. Nobre, R. J. Haarsma, and E. J. D. Campos, 2007: Negative ocean-atmosphere feedback in the South Atlantic Convergence Zone. Geophys. Res. Lett., 34, 18, L18809, doi: 10.1029/2007GL030401.

Delire C., Foley, J.A., Thompson, S. 2002. Evaluating the carbon cycle of a coupled atmosphere-biosphere model. Global Biogeochemical Cycles 17: 1012, DOI:10. 1029/2002 GB001870.

Dias, L. C. P., Pimenta, F. M., Santos, A. B., Costa, M. H., Ladle, R. J., 2016. Patterns of land use, extensification and intensification of Brazilian agriculture. Global Change Biology, in press. doi: 10.1111/gcb.13314

Dirmeyer, P. A., and K. L. Brubaker, 2007: Characterization of the Global Hydrologic Cycle from a Back-Trajectory Analysis of Atmospheric Water Vapor. J. Hydrometeor., 8, 20–37, doi: 10.1175/JHM557.1.

Drumond, A., J. Marengo, T. Ambrizzi, R. Nieto, L. Moreira, and L. Gimeno, 2014: The role of the Amazon Basin moisture in the atmospheric branch of the hydrological cycle: A Lagrangian analysis. Hydrol. Earth Syst. Sci., 18, 2577–2598, doi: 10.5194/hess-18-2577-2014.

Durán-Quesada, A. M., M. Reboita, L. Gimeno, 2012: Precipitation in tropical America and the associated sources of moisture: a short review. Hydrol. Sci. J., 57, 4, 612–624, doi: 10.1080/02626667.2012.673723.

Eltahir, E.A.B., and R.L. Bras, 1994: Precipitation recycling in the Amazon basin. Quarterly journal of the royal meteorological society, 120, 861-80.

Eltahir, E. A. B. and Bras, R. L.: Precipitation recycling, Rev. Geophys., 34, 367–378, 1996.

Eltahir E.A.B., 1996: Role of vegetation in sustaining large-scale atmospheric circulations in the tropics. J. Geophys. Res., 101, 4255–4268.

Foley, J.A., Prentice, I.C., Ramankutty, N., Levis, S., Pollard, D., Sitch, D., Haxeltine, A. 1996. An integrated biosphere model of land surface processes, terrestrial carbon balance, and vegetation dynamics. Global Biogeochemical Cycles 10: 603–628.

Foley, J. A., and Coauthors, 2005: Review Global Consequences of Land Use. Sci., 309, 570–575, doi: 10.1126/science.1111772.

Gimeno, L., A. Drumond, R. Nieto, R. M. Trigo, and A. Stohl, 2010: On the origin of continental precipitation. Geophys. Res. Lett., 37, 13, doi: 10.1029/2010GL043712.

Gimeno, L., A. Stohl, R. M. Trigo, F. Dominguez, K. Yoshimura, L. Yu, A. Drumond, A. M. Durn-Quesada and R. Nieto, 2012: Oceanic And Terrestrial Sources Of Continental Precipitation. Rev. Geophys. 50, RG4003 .

Goessling, H., and Reick, C. H., 2013. On the" well-mixed" assumption and numerical 2-D tracing of atmospheric moisture. Atmospheric Chemistry and Physics, 13, 5567-5585. doi:10.5194/acp-13-5567-2013

Hansen, M. C. and Coauthors, 2013: High-Resolution global maps of 21st-century forest cover change. Sci., 342, 850–853, doi: 10.1126/science.1244693.

Henderson-Sellers, A., K. McGuffie, and H. Zhang, 2002: Stable isotopes as validation tools for global climate model predictions of the impact of Amazonian deforestation. J. Climate, 15, 18, 2664–2677, doi: 10.1175/1520-0442(2002)015.

Imbuzeiro HMA. 2005. Calibration of the IBISmodel in the Amazonian forest using multiple sites. Unpublished MS Thesis (in Portuguese with abstract in English), Federal University of Vi¸cosa, Vi¸cosa, 67pp.

Keys, P. W., Wang-Erlandsson, L., Gordon, L. J. 2016. Revealing Invisible Water: Moisture Recycling as an Ecosystem Service. PloS one, 11(3), e0151993.

Kiehl JT, Hack JJ, Bonan GB, Boville BA, Williamson DL, Rasch PJ. 1998. The National Center for Atmospheric Research Community Climate Model: CCM3. Journal of Climate 11: 1131–1149.

Ladle, R. J., A. C. M. Malhado, P. A. Tood, and A. C. M. Malhado, 2010: Perceptions of Amazonian deforestation in the British and Brazilian media. Acta Amazonica, 40, 2, 319–324, doi: 10.1590/S0044-59672010000200010.

Lapola, D. M., and Coauthors, 2013: Pervasive transition of the Brazilian land-use system. Nature Climate Change, 4, 1, 27–35, doi: 10.1038/nclimate2056.

Lawrence, D., and K. Vandecar, 2014: The impact of tropical deforestation on climate and links to agricultural productivity. Nature Climate Change, 5, 27-36, doi: 10.1038/nclimate2430.

Marengo, J. A., and Coauthors, 2012: Recent developments on the South American monsoon system. Int. J. Climatol., 32, 1, 1–21, doi: 10.1002/joc.2254.

Martinez, J. A., and F. Dominguez, 2014: Sources of Atmospheric Moisture for the La Plata River Basin. J. Climate, 27, 6737-6753, doi: 10.1175/JCLI-D-14-00022.1.

Misra, V., 2008: Coupled Air, Sea, and Land Interactions of the South American Monsoon. J. Climate, 21, 23, 6389–6403, doi: 10.1175/2008JCLI2497.1.

Nobre, P., M. Malagutti, D. F. Urbano, R. A. F. de Ameida, and E. Giarolla, 2009: Amazon deforestation and climate change in a coupled model simulation. J. Climate, 22, 5686–5697, doi: 10.1175/2009JCLI2757.1.

Oliveira, L. J. C., M. H. Costa, B. S. Soares-Filho, and M. T. Coe, 2013: Large-scale expansion of agriculture in Amazonia may be a no-win scenario. Environ. Res. Lett., 8, 2, 024021, doi: 10.1088/1748-9326/8/2/024021.

Paegle, J. N., and K. C. MO, 2002: Linkages between summer rainfall variability over South America and sea surface temperature anomalies. J. Climate, 15, 12, 1389–1407, doi: 10.1175/1520-0442(2002)015.

Pires, G. F., and M. H. Costa, 2013: Deforestation causes different subregional effects on the Amazon bioclimatic equilibrium. Geophys. Res. Lett., 40, 14, 3618–3623, doi: 10.1002/grl.50570.

Pires, G. F.; Abrahão, G. M. ; Brumatti, L. M. ; Oliveira, L. J.C. ; Costa, M. H. ; Liddicoat, S. ; Kato, E. ; Ladle, R. J.2016 . Increased climate risk in Brazilian double cropping agriculture systems: Implications for land use in Northern Brazil. Agricultural and Forest Meteorology, 228-229, 286-298. doi:10.1016/j.agrformet.2016.07.005

Richter, I., C. R. Mechoso, and A. W. Robertson, 2007: What determines the position and intensity of the South Atlantic anticyclone in austral winter ? - An AGCM study. J. Climate, 21, 214-229, doi: 10.1175/2007JCLI1802.1.

Roy, S. B., and R. Avissar, 2002: Impact of land use/land cover change on regional hydrometeorology in Amazonia. J. Geophys. Res., 107, D20, 1–12, doi: 10.1029/2000JD000266.

Sampaio, G., C. Nobre, M. H. Costa, P. Satyamurty, B. S. Soares-Filho, and M. Cardoso, 2007: Regional climate change over eastern Amazonia caused by pasture and soybean cropland expansion. Geophys. Res. Lett., 34, 17, L17709, doi: 10.1029/2007GL030612.

Satyamurty, P., C. P. W. Da Costa, and A. O. Manzi, 2012: Moisture source for the Amazon Basin: a study of contrasting years. Theoretical and Appl. Climatol., 111, 1-2, 195–209, doi: 10.1007/s00704-012-0637-7.

Senna, M.C.A., Costa, M. H, Pires, G.F. Vegetation-atmosphere-soil nutrient feedbacks in the Amazon for different deforestation scenarios.2009. Journal of Geophysical Research, v. 114, D04104. doi:10.1029/2008JD010401.

Silva, A. E., and L. M. V. Carvalho, 2007: Large-scale index for South America Monsoon. Atmos. Sci. Lett., 8, 51-57, doi: 10.1002/asl.150.

Silva, V. B. S., and V. E. Kousky, 2012: The South American Monsoon System: Climatology and Variability. Mod. Climatol., 398, doi: 10.5772/2014.

Soares-Filho B. S., and Coauthors, 2006: Modelling conservation in the Amazon Basin. Nature, 440, 520-523, doi: 10.1038/nature04389.

Spracklen, D. V., S. R. Arnold, and C. M. Taylor, 2012: Observations of increased tropical rainfall preceded by air passage over forests. Nature, 489, 7415, 282–5, doi: 10.1038/nature11390.

Spracklen, D. V., and Garcia-Carreras, L. 2015. The impact of Amazonian deforestation on Amazon basin rainfall. Geophysical Research Letters, 42(21), 9546-9552.

Stickler, C. M., M. T. Coe, M. H. Costa, D. C. Nepstad, D. G. McGrath, L. C. P. Dias, H. O. Rodrigues, and B. S. Soares-Filho, 2013: Dependence of hydropower energy generation on forests in the Amazon Basin at local and regional scales. Proc. Natl. Acad. Sci. USA, 110, 23, 9601–6, doi: 10.1073/pnas.1215331110.

Stohl, A., P. A. James, 2004: Lagrangian Analysis of the Atmospheric Branch of the Global Water Cycle. Part I: Method Description, Validation, and Demonstration for the August 2002 Flooding in Central Europe. J. Hydrometeor., 5, 4, 656–678, doi: 10.1175/1525-7541(2004)005.

Stohl, A., P A James, 2005: Lagrangian Analysis of the Atmospheric Branch of the Global Water Cycle. Part II: Moisture Transports between Earth's Ocean Basins and River Catchments. J. Hydrometeor., 6, 6, 961–984, doi: 10.1175/JHM470.1.

Swann, A. L., Longo, M., Knox, R. G., Lee, E., Moorcroft, P. R. 2015. Future deforestation in the Amazon and consequences for South American climate. Agricultural and Forest Meteorology, 214, 12-24.

van der Ent, R. J., H. H. G. Savenije, B. Schaefli, and S. C. Steele-Dunne, 2010: Origin and fate of atmospheric moisture over continents. Water Resour. Res., 46, 1–12, doi: 10.1029/2010WR009127.

Van der Ent, R.J. and H.H.G. Savenije. Length and time scales of atmospheric moisture recycling. Atmos. Chem. Phys., 11, 1853–1863, 2011. doi:10.5194/acp-11-1853-2011

Vera, C., and Coauthors, 2005: Toward a Unified View of the American Monsoon Systems. J. Climate, 19, 4977-5000, doi: 10.1175/JCLI3896.1.

Table 1 - Annual mean evapotranspiration (mm/day) for different sites in the Amazon rainforest simulated by CCM3-IBIS and as reported by Costa et al. (2010).

	Annual mean evapotranspiration (mm/day)		
	Costa et al. (2010)	CCM3-IBIS control run	e (%)
Manaus 60°13′W 2°36′S	3.58	5.18	30.89
Santarem 54°58′W 2°51′S and 54°57′W 3°03′S	3.49	3.28	-6.40
Jaru 61°56′W 10°46′S	3.57	4.43	19.41
Sinop 55°19′W 11°25′S	3.11	3.84	19.01

Figure captions:

Figure 1. Orientation map showing the soybean area in Mato Grosso and the Madeira and Xingu basins with potential for hydropower generation.

Figure 2. Deforestation scenarios used in simulations. a) A0 is the control simulation which considers forest biome intact, b) A20 is equivalent to 20% of deforestation, and so on (Pires and Costa 2013).

Figure 3. Simulated (Sim), Observed (Obs) and Simulation error (Sim-Obs) of seasonal mean precipitation (mm day^{-1}) from 1961 to 1990.

Figure 4. Source of water vapor (mm month^{-1}) that precipitates over the Xingu basin and Evapotranspiration (mm month^{-1}) for SON and DJF. P is the average precipitation in the region (mm month^{-1}); E is the average evapotranspiration (mm month-1); ΔP is the difference in precipitation in the region between each deforested scenario (F20, F40 and F60) and control scenario (F0), in mm month^{-1}; IWT are the vectors of the vertically integrated water vapor transport for the F0 scenario in (a) SON and (j) DJF. Panels (c) to (i) are the changes in the contribution of each pixel from that in the control simulation (panel b) in the SON trimester and panels (l) to (r) are the changes in the contribution of each pixel from that in the control simulation (panel k) the DJF trimester. The sum of all colored pixels is equal to P. Rather than showing the ocean contribution in a spatially explicit way, here we chose to condense all ocean contributions as originating from the land-surface grid cell directly adjacent to the ocean. The thicker black line is the Xingu River basin. Black dots indicate *pixels where the ensemble mean water vapor transport is significantly different according to Student's t test* (α=5%, n=4).

Figure 5. Source of water vapor (mm month^{-1}) that precipitates over the Madeira basin and Evapotranspiration (mm month^{-1}) for SON and DJF. P is the average precipitation in the region (mm month^{-1}); E is the average evapotranspiration (mm month-1); ΔP is the difference in precipitation in the region between each deforested scenario (F20, F40 and F60) and control scenario (F0), in mm month^{-1}; IWT are the vectors of the vertically integrated water vapor transport for the F0 scenario in (a) SON and (j) DJF. Panels (c) to (i) are the changes in the contribution of each pixel from that in the control simulation (panel b) in the SON trimester and panels (l) to (r) are the changes in the contribution of each pixel from that in the control simulation (panel k) the DJF trimester. The sum of all colored pixels is equal to P. Rather than showing the ocean contribution in a spatially explicit way, here we chose to condense all ocean contributions as originating from the land-surface grid cell directly adjacent to the ocean. The thicker black line is the Madeira River basin. Black dots indicate *pixels where the ensemble mean water vapor transport is significantly different according to Student's t test* (α=5%, n=4).

Figure 6. Source of water vapor (mm $month^{-1}$) that precipitates over the soybean producing region in Mato Grosso and Evapotranspiration (mm $month^{-1}$) for SON and DJF. P is the average precipitation in the region (mm $month^{-1}$); E is the average evapotranspiration (mm $month^{-1}$); ΔP is the difference in precipitation in the region between each deforested scenario (F20, F40 and F60) and control scenario (F0), in mm $month^{-1}$; IWT are the vectors of the vertically integrated water vapor transport for the F0 scenario in (a) SON and (j) DJF. Panels (c) to (i) are the changes in the contribution of each pixel from that in the control simulation (panel b) in the SON trimester and panels (l) to (r) are the changes in the contribution of each pixel from that in the control simulation (panel k) the DJF trimester. The sum of all colored pixels is equal to P. Rather than showing the ocean contribution in a spatially explicit way, here we chose to condense all ocean contributions as originating from the land-surface grid cell directly adjacent to the ocean. The thicker black line is soybean producing region in Mato Grosso. Black dots indicate *pixels where the ensemble mean water vapor transport is significantly different according to Student's t test* (α=5%, n=4).

Figure 7 – Changes in (a) power generation in Belo Monte and (b) soybean production in Mato Grosso due to Amazon deforestation.

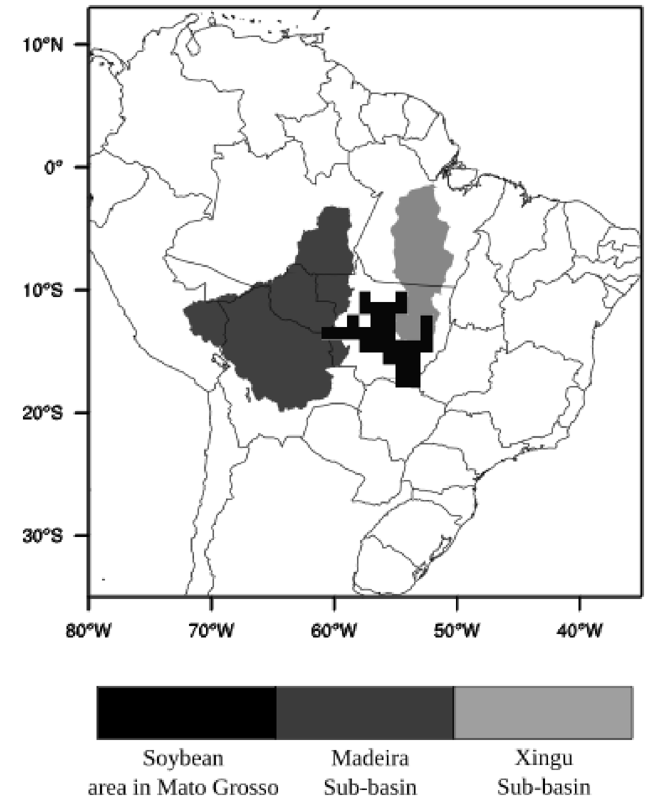

Figure 1. Orientation map showing the soybean area in Mato Grosso and the Madeira and Xingu basins with potential for hydropower generation.

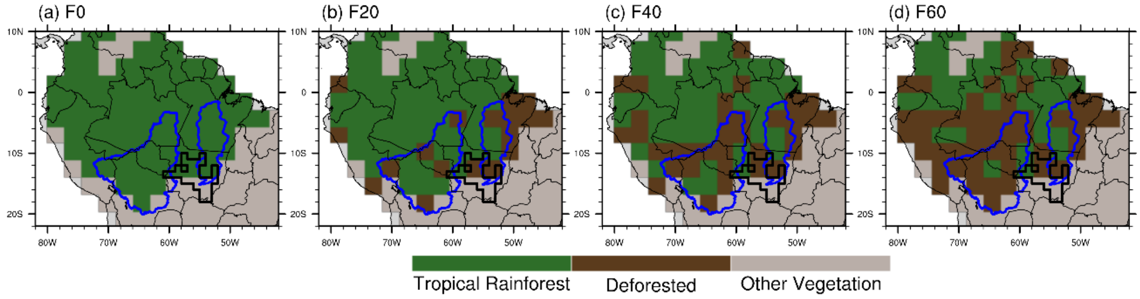

Figure 2. Deforestation scenarios used in simulations. a) F0 is the control simulation which considers forest biome intact, b) F20 is equivalent to 20% of deforestation, and so on (Pires and Costa 2013). Blue lines indicate the Xingu and Madeira basins. Black thick line indicate the soybean planted area in Mato Grosso.

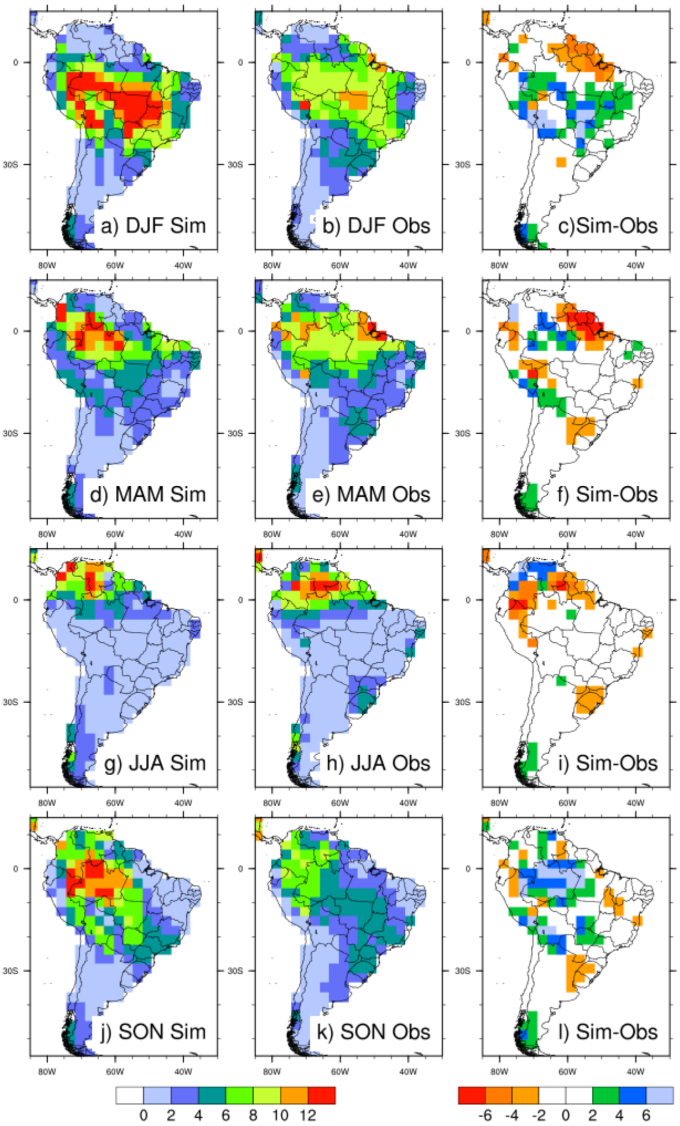

Figure 3. Simulated (Sim), Observed (Obs) and Simulation error (Sim-Obs) of seasonal mean precipitation (mm day^{-1}) from 1961 to 1990.

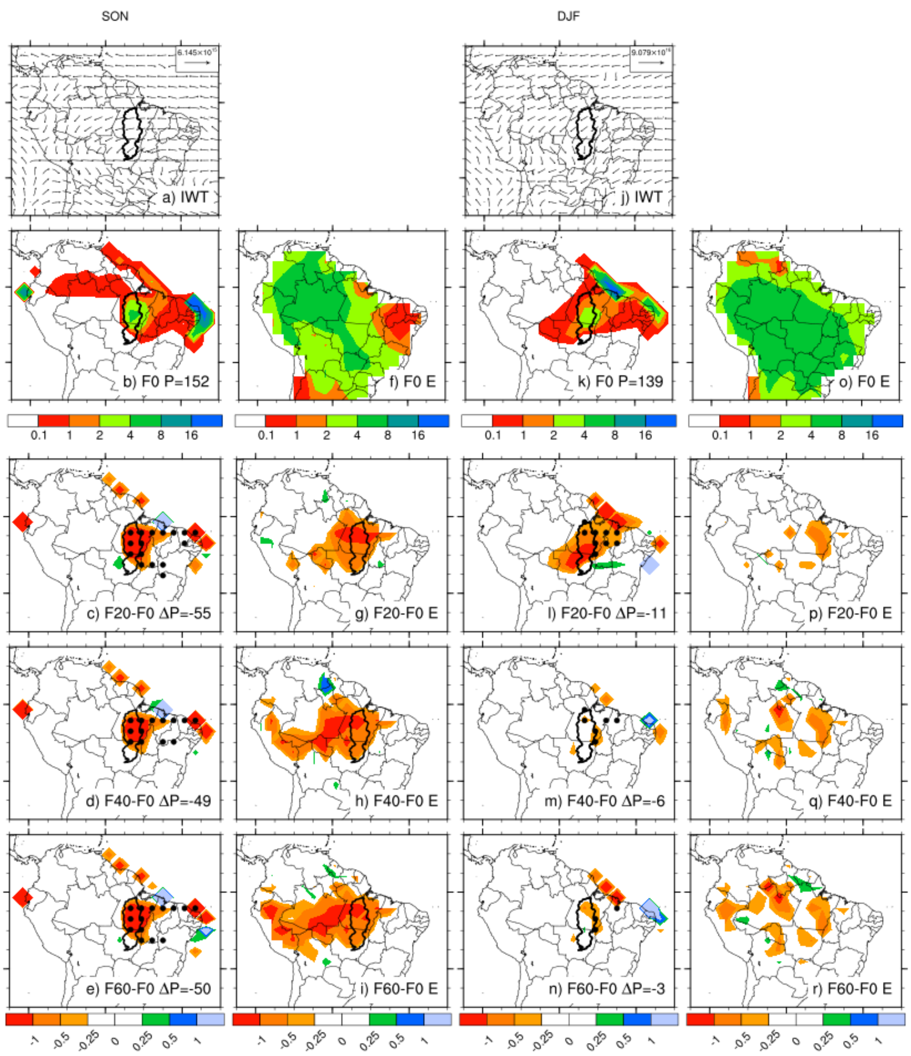

Figure 4. Source of water vapor (mm month^{-1}) that precipitates over the Xingu basin and Evapotranspiration (mm month^{-1}) for SON and DJF. P is the average precipitation in the region (mm month^{-1}); E is the average evapotranspiration (mm month^{-1}); ΔP is the difference in precipitation in the region between each deforested scenario (F20, F40 and F60) and control scenario (F0), in mm month^{-1}; IWT are the vectors of the vertically integrated water vapor transport for the F0 scenario in (a) SON and (j) DJF. Panels (c) to (i) are the changes in the contribution of each pixel from that in the control simulation (panel b) in the SON trimester and panels (l) to (r) are the changes in the contribution of each pixel from that in the control simulation (panel k) the DJF trimester. The sum of all colored pixels is equal to P. Rather than showing the ocean contribution in a spatially explicit way, here we chose to condense all ocean contributions as originating from the land-surface grid cell directly adjacent to the ocean. The thicker black line is the Xingu River basin. Black dots indicate *pixels where the ensemble mean water vapor transport is significantly different according to Student's t test* (α=5%, n=4).

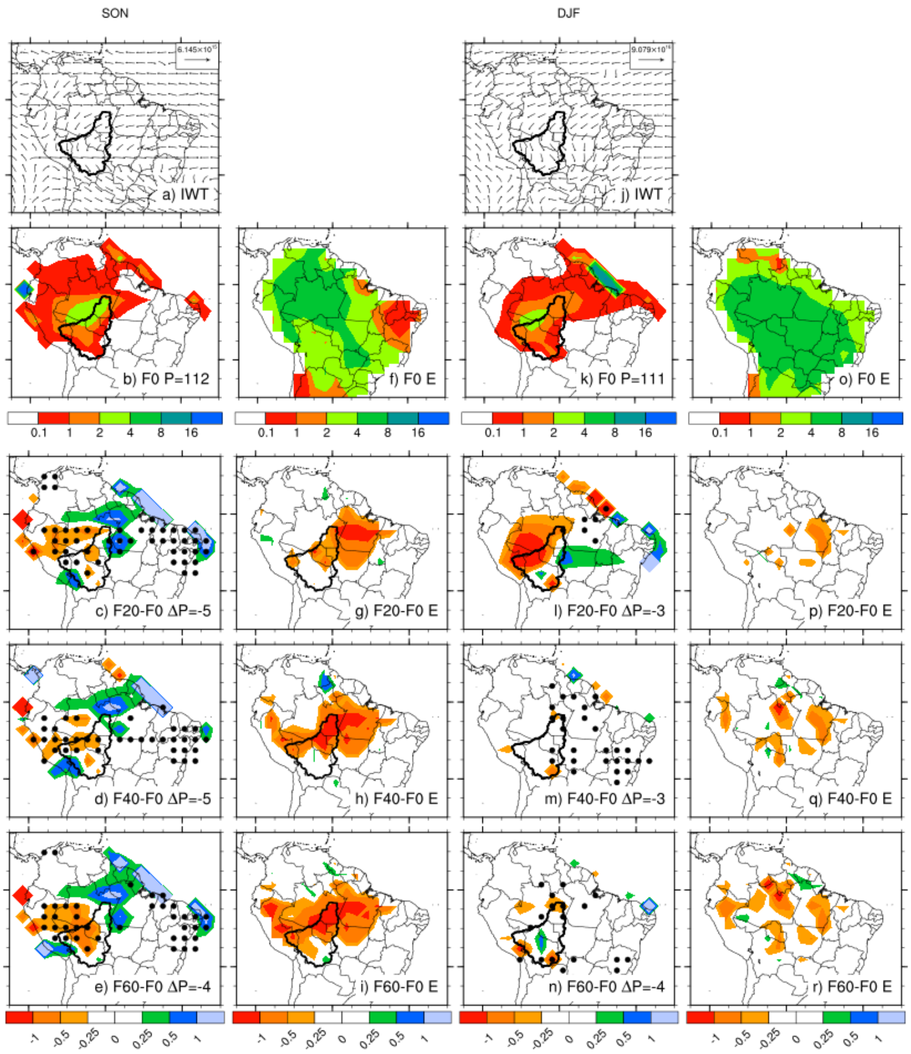

Figure 5. Source of water vapor (mm month^{-1}) that precipitates over the Madeira basin and Evapotranspiration (mm month^{-1}) for SON and DJF. P is the average precipitation in the region (mm month^{-1}); E is the average evapotranspiration (mm month^{-1}); ΔP is the difference in precipitation in the region between each deforested scenario (F20, F40 and F60) and control scenario (F0), in mm month^{-1}; IWT are the vectors of the vertically integrated water vapor transport for the F0 scenario in (a) SON and (j) DJF. Panels (c) to (i) are the changes in the contribution of each pixel from that in the control simulation (panel b) in the SON trimester and panels (l) to (r) are the changes in the contribution of each pixel from that in the control simulation (panel k) the DJF trimester. The sum of all colored pixels is equal to P. Rather than showing the ocean contribution in a spatially explicit way, here we chose to condense all ocean contributions as originating from the land-surface grid cell directly adjacent to the ocean. The thicker black line is the Madeira River basin. Black dots indicate *pixels where the ensemble mean water vapor transport is significantly different according to Student's t test* (α=5%, n=4).

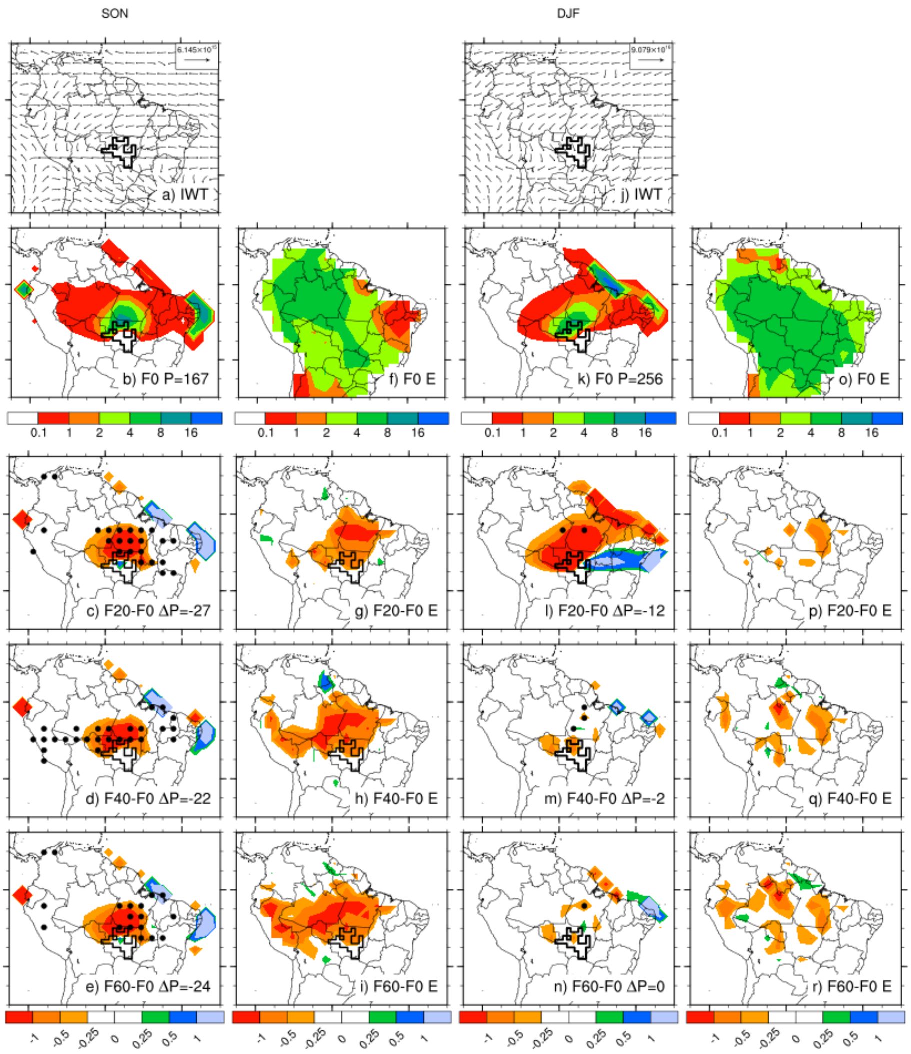

Figure 6. Source of water vapor (mm month^{-1}) that precipitates over the soybean producing region in Mato Grosso and Evapotranspiration (mm month^{-1}) for SON and DJF. P is the average precipitation in the region (mm month^{-1}); E is the average evapotranspiration (mm month^{-1}); ΔP is the difference in precipitation in the region between each deforested scenario (F20, F40 and F60) and control scenario (F0), in mm month^{-1}; IWT are the vectors of the vertically integrated water vapor transport for the F0 scenario in (a) SON and (j) DJF. Panels (c) to (i) are the changes in the contribution of each pixel from that in the control simulation (panel b) in the SON trimester and panels (l) to (r) are the changes in the contribution of each pixel from that in the control simulation (panel k) the DJF trimester. The sum of all colored pixels is equal to P. Rather than showing the ocean contribution in a spatially explicit way, here we chose to condense all ocean contributions as originating from the land-surface grid cell directly adjacent to the ocean. The thicker black line is soybean producing region in Mato Grosso. Black dots indicate *pixels where the ensemble mean water vapor transport is significantly different according to Student's t test* (α=5%, n=4).

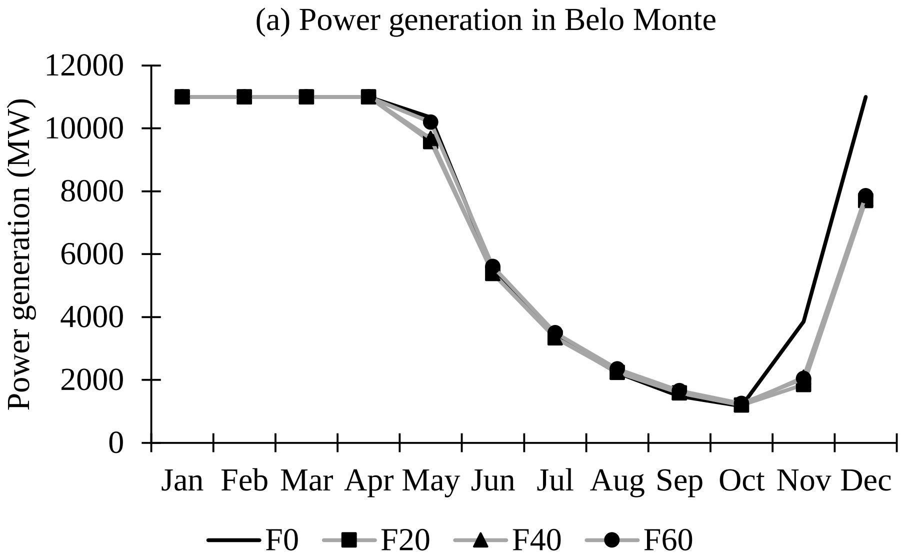

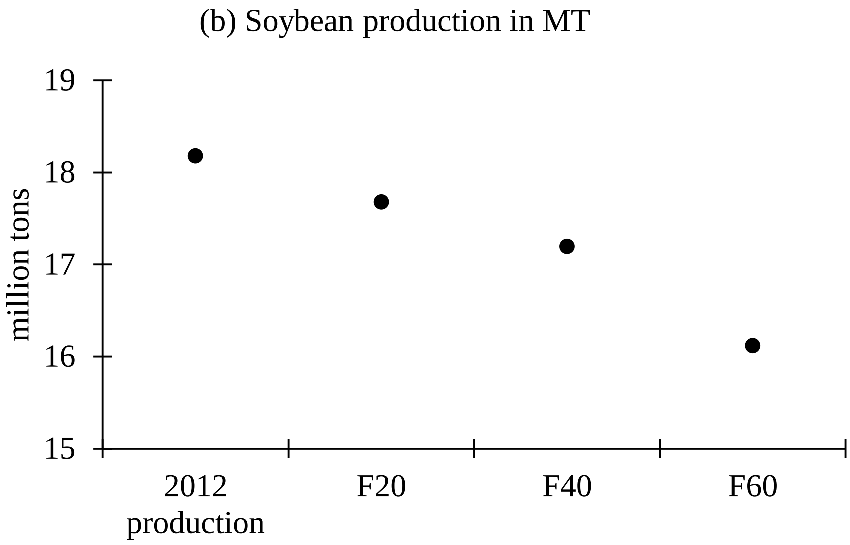

Figure 7 – Changes in (a) power generation in Belo Monte and (b) soybean production in Mato Grosso due to Amazon deforestation.